The Journal of the Astronautical Sciences (2026) 73:25
https://doi.org/10.1007/s40295-025-00568-6

RESEARCH

High-Accuracy Mass Estimation of Small Asteroids for Planetary Defense Using the Gravity Imaging Radio Observer (GIRO)

Edoardo Gramigna[1,2] · Ryan S. Park[1] · Joseph E. Riedel[1] · Andrea Magnanini[1,3] · Steven R. Chesley[1] · Davide Farnocchia[1] · Paolo Tortora[2,3] · Marco Zannoni[2,3]

Received: 31 August 2025 / Accepted: 16 December 2025

Abstract

Accurate mass determination of small, sub-kilometer asteroids is a key challenge in planetary defense, particularly for newly discovered potentially impacting asteroids requiring rapid response. This work investigates the Gravity Imaging Radio Observer (GIRO), an innovative instrument concept based on inter-satellite Doppler tracking between a host spacecraft and small radio probes, combined with high-precision optical imaging using the Advanced Pointing Imaging Camera. We assess GIRO's performance in a simulated flyby mission targeting asteroid 2024 YR4, and demonstrate that a compact beacon-based architecture can achieve formal 1σ mass-estimation uncertainties of about 20% for a 60-meter-class object, assuming a Bennu-like density and a flyby at 50 m altitude above the surface with a relative velocity of 5 km/s. Most of the information content arises from post-encounter differential deflections between the host spacecraft and beacons, allowing robust estimation even in scenarios with limited data availability around closest approach. Sensitivity studies confirm that the technique is resilient to variations in flyby geometry and beacon release strategy, enabling accurate mass determination for a wide range of asteroid sizes, flyby velocities, and operational constraints. These findings position GIRO, in combination with a capable imager, as a highly promising candidate for planetary defense and reconnaissance missions requiring rapid deployment, minimal complexity, and reliable scientific and engineering return.

Keywords Small bodies · Planetary defense · Asteroid · PHA · Mass estimation · Gravity imaging radio observer · GIRO · Gravity science · Inter-satellite range rate · Radio beacon · Orbit determination

Extended author information available on the last page of the article

Published online: 02 March 2026

1 Introduction

Understanding the gravity field of planetary bodies is a cornerstone of planetary science as it provides key insights into their internal structure, composition, formation history, and dynamical evolution [43, 44, 58]. This field of study, often referred to as gravity science, relies heavily on high-precision radiometric measurements, particularly Doppler (i.e., range-rate) tracking, enabled by ground-based radio antennas such as NASA's Deep Space Network (DSN) and ESA's Tracking Station Network (ESTRACK) [54].

Gravity science plays a vital role across planetary missions, from mapping large bodies such as Mercury, Venus, the Moon, Mars, and the gas giants, to characterizing the mass and internal properties of small irregular objects like comets and asteroids [43, 49]. In these contexts, gravity estimation techniques not only help determine bulk properties like mass and density, but also reveal subtle features of subsurface structure or mass distribution anomalies, which are otherwise inaccessible through remote sensing.

In the specific context of planetary defense, precise knowledge of an asteroid's mass becomes especially critical because it informs impact risk assessments, and aids in the design of mitigation missions. This is particularly relevant for Potentially Hazardous Asteroids (PHAs), a subset of Near-Earth Asteroids (NEAs) characterized by minimum orbit intersection distances with Earth of less than 0.05 au and diameters greater than 140 m [12, 22, 34] (see Fig. 1), as well as smaller potentially impacting asteroids. Due to their size and proximity, these objects can pose significant threats

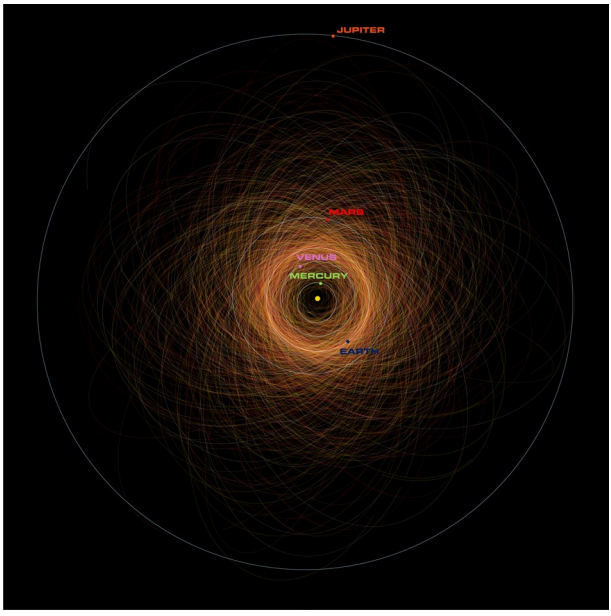

Fig. 1 Overview of the known orbits of the 887 numbered PHAs in the inner solar system. The plot shows a dense and dynamically complex environment, including planet-crossing, Earth-crossing, and resonant regions. PHAs orbital data sourced from [38]

in the event of an Earth impact, making their physical characterization a high priority for planetary defense initiatives [39, 47].

Despite advances in observational techniques, determining the mass of small bodies, particularly those under 1 km in diameter, via single-spacecraft flybys remains a significant challenge. The primary difficulty lies in the extremely weak gravitational pull exerted by such bodies, which induces only subtle perturbations to a spacecraft's trajectory, often below the sensitivity threshold of traditional flyby tracking techniques. Ground-based estimation is further complicated by uncertainties in tracking geometry and signal propagation through Earth's atmosphere and interplanetary media [1].

Although orbiters can, and have, successfully measured the mass and gravity fields of small asteroids, including those less than 1 km in diameter (e.g., Chesley et al. [13]; Gramigna et al. [23]; Scheeres et al. 50; Pätzold et al. [41]), flybys have not yet achieved comparable success. The short duration of the gravitational interaction, combined with the high relative velocity, limits the sensitivity to perturbations and demands alternative approaches to extract mass-related information effectively.

To address this limitation, this study investigates the Gravity Imaging Radio Observer (GIRO), an innovative instrument concept based on inter-satellite radio links [45], designed to operate in conjunction with a high-resolution imager, such as the Advanced Pointing Imaging Camera (APIC) [46]. GIRO builds on the heritage of previous missions that have demonstrated the effectiveness of inter-spacecraft tracking–namely GRACE and GRACE-FO, which monitored Earth's time-variable gravity field [3, 32, 55], and GRAIL, which employed twin lunar orbiters to map the Moon's interior in exceptional detail [30, 58, 59]. This heritage will be further extended by ESA's Hera mission, which will track two CubeSats in the Didymos system beginning in late 2026 [21, 23].

Specifically, GIRO adapts the core principle of these missions, high-precision inter-satellite Doppler tracking, to a broader range of mission scenarios. GIRO's beacon-based architecture is designed to support both detailed gravity field recovery of planetary bodies and accurate mass determination of small planetary bodies during rapid-response flybys or short-duration rendezvous. This versatility makes GIRO particularly well-suited for planetary defense applications, where flexibility, simplicity, and rapid deployment are essential.

In the context of asteroid mass determination using GIRO, one or more small probes, equipped with radio beacons but no propulsion, are released from a host spacecraft hours before the encounter. Depending on mission requirements, these probes may serve as free-flying inertial references during a close flyby by the host spacecraft, or conversely, be sent on close approaches themselves and tracked by the host spacecraft. After release, they are tracked using high-precision Doppler and APIC optical measurements (to determine their spin states) by the host spacecraft. The resulting inter-satellite tracking dataset, free from atmospheric distortion and independent of Earth-spacecraft geometry, enables the precise reconstruction of gravitational deflections, and hence the estimation of asteroid mass.

Asteroid 2024 YR4, initially identified as a potential impactor due to its predicted close approach to Earth in 2032, serves as a motivating example for this work [19, 48]. Although follow-up observations eventually ruled out an impact risk to Earth

[27], the case highlights the critical need for rapid-response capabilities able to physically characterize NEOs shortly after discovery. While ground-based tracking is generally sufficient for orbit determination, key physical parameters such as mass often remain poorly constrained–limiting our ability to assess potential impact energy and plan effective mitigation strategies.

This study evaluates the performance of the GIRO system in a simulated flyby mission targeting asteroid 2024 YR4. The analysis investigates the achievable uncertainty in the mass estimate using inter-satellite Doppler and APIC optical tracking under realistic mission conditions, and demonstrates the technical feasibility and operational flexibility of the GIRO concept in support of planetary defense.

This paper is structured as follows: Sect. 2 presents the motivation for this work. Section 3 introduces the GIRO system and its key technological elements. Section 4 reviews mass estimation techniques for spacecraft flybys. Section 5 describes the flyby operations concept and probe deployment strategy. Section 6 outlines the orbit determination framework, including the dynamical, measurement, and maneuver models. Section 7 presents simulation results for the 2024 YR4 case, as well as for a broader set of asteroid and flyby conditions. Finally, Sect. 8 summarizes the findings and discusses implications for planetary defense.

2 Motivation

The case of 2024 YR4 highlights a critical limitation in current planetary defense infrastructure: the absence of space-based systems capable of providing rapid and accurate mass measurements for newly discovered potentially impacting asteroids. Mass is a key input for determining the kinetic energy of a potential impactor and directly affects modeled impact consequences such as surface damage, atmospheric disruption, and tsunami generation [11, 39]. Equally important is an understanding of internal structure and porosity, which govern how an asteroid responds to impulsive deflection methods [24, 25, 51]. Despite their importance, both mass and porosity remain difficult to constrain from ground-based or flyby observations. Rendezvous missions provide accurate measurements but require long preparation times and high costs, incompatible with the rapid reaction demanded by planetary defense. This motivates the development of new mission concepts–such as the GIRO architecture–designed to bridge this capability gap.

To address this need, we investigate a distributed mission architecture involving a primary platform (the host spacecraft) that carries and deploys a set of semi-active radio beacons known as GIROs. These beacons are released prior to the encounter to support high-precision tracking. Building on prior studies such as [5, 14] and [6], which explored flyby-based mass estimation, we adopt a novel configuration that leverages unprecedented Doppler-optical tracking accuracy and an alternative operational strategy: the GIRO probes serve as distant inertial references while the main spacecraft performs a controlled close flyby of the asteroid. This setup minimizes operational risks, exploits spacecraft autonomy, and enables favorable tracking geometries for precise mass determination. In our concept, the high precision of GIRO Doppler measurements is the key driver for improving the asteroid GM esti-

mation, as GIRO range-rate data tightly constrain the gravitational interaction during the flyby. Complementarily, optical images provide an independent constraint on the relative geometry and attitude between the spacecraft and the asteroid, ensuring a well-determined flyby trajectory and enabling a robust dynamical reconstruction.

A flyby reconnaissance mission of a small body is expected to be equipped with an imaging system, typically both visible and thermal cameras. Depending on the target's size, rotational state, and observing geometry, it is anticipated that the volume can be estimated with an accuracy 10–30% [8]. By enabling reliable estimates of mass and, indirectly, porosity, derived from the combination of mass and shape measurements, the proposed system contributes a crucial capability to future planetary defense missions. In particular, shape information can be obtained through onboard imaging, allowing for improved density and porosity assessments. In turn, this enables more accurate threat evaluation and better-informed mitigation planning, even under tight time constraints.

3 Gravity Imaging Radio Observer

GIRO is a novel gravity science instrument designed to enable high-precision mass and gravity field estimation of planetary bodies, including small asteroids, using high-accuracy inter-satellite Doppler measurements [45]. It can optionally be operated alongside a high-resolution imager, such as APIC, to enhance scientific return [46].

Each GIRO unit is a compact, battery-powered radio beacon equipped with a coherent X-band transponder that communicates with a host spacecraft to provide range-rate measurements with precision expected to be at least as good as $\leq 1\mu\mathrm{m/s}$ over 60-second intervals. This is 10 to 100 times more accurate than the capabilities of conventional Earth-based tracking and comparable to the baseline pre-launch performance expected of the GRAIL mission (which in flight greatly exceeded this level) [29].

The probes are spin-stabilized, and by orienting GIRO's spin axis normal to the host spacecraft-GIRO velocity direction, spacecraft thermal re-radiation[1] acting in the plane perpendicular to the spin axis is effectively averaged out. The residual component along the spin axis can be largely canceled by flying two GIROs simultaneously, using differential measurements to isolate the gravitational signal of interest. Each probe is equipped with an analog, carrier-only transponder to maintain frequency coherence while minimizing system complexity. Each unit also features LED beacons for optical tracking and spin-state determination, enabling combined Doppler-optical gravity estimation. The GIROs can be optically tracked using the APIC camera onboard the host spacecraft, a compact, dual-imager system designed for planetary geodesy and precision navigation [46]. APIC provides simultaneous imaging of surface targets, bodies, and star fields, delivering high-precision pointing knowledge ($\sim$0.25 pixel, approximately 1 arcsecond for both the narrow and

[1] Spacecraft thermal re-radiation affects spacecraft orbits when a net recoil force results from the uneven emission of radiation from the spacecraft surface; these forces can perturb spacecraft trajectories.

wide-angle cameras). Finally, the use of Commercial Off-The-Shelf (COTS) components makes GIRO a cost-effective and scalable solution for rapid-response planetary defense missions.

As demonstrated by [45], the GIRO concept can support a variety of planetary science investigations. Deploying the probes closer to target bodies enables the determination of high-order spherical harmonic coefficients and insights into the interior structure, such as those of the Moon, the gas and icy giants and their moons, as well as their tidal parameters and precise orbital solutions, all with unprecedented accuracy. Moreover, using the beacons to perform flybys of small bodies, or as free-space references, allows for high-precision estimates of an asteroid's mass and potentially its gravity field. Two primary mission architectures have been proposed for deploying GIROs during asteroid flybys [45]:

- In the first approach, GIROs are released shortly before the flyby, forming a spatial "cloud" around the asteroid, similar to Christensen et al. [14]; Hesar et al. [26]; Atchison et al. [4]. Each probe independently samples the gravity field during its passage, and the asteroid's mass is estimated from the collective deflection signatures extracted from optical and Doppler tracking during and after the flyby.
- In the second approach, adopted in this study, the probes are released 6-12 h before the encounter and remain in safer, more distant trajectories, acting as inertial free-space references. The host spacecraft performs a close, autonomous flyby and experiences the primary gravitational perturbation, which is then measured relative to the GIROs. Figure 2 shows an artistic impression of this concept, including the assumed measurements for this investigation.

The first approach, i.e. releasing probes on ballistic trajectories toward the asteroid, has inherent limitations. Since the probes cannot be maneuvered once deployed,

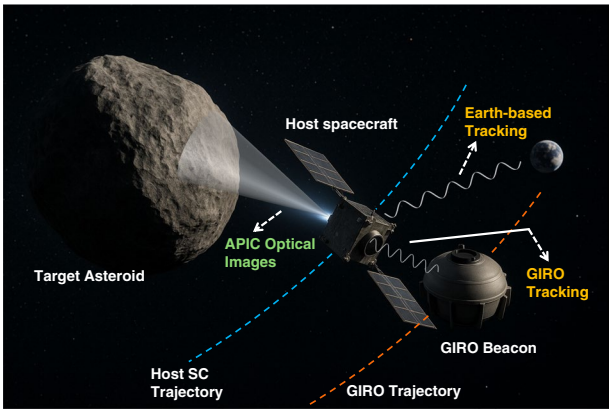

Fig. 2 Artistic impression of the proposed mission scenario and measurement concept. The host spacecraft performs a close flyby of the target asteroid, while one or more GIRO beacons serve as inertial reference points in free space. The measurements include APIC optical images of the asteroid, Earth-based radiometric tracking, and GIRO Doppler data. For clarity, the GIRO beacon is not shown to scale, its actual diameter is 50 cm

their trajectories cannot be actively targeted or corrected. Mission success therefore depends on the natural dispersion of the probes' ballistic paths, which is governed by mechanical release uncertainties typically around 5% of the line-of-sight release velocity (expected to be around 1 m/s). This results in a position uncertainty cloud spanning hundreds of meters by Closest Approach (CA). Consequently, this strategy relies on the probability that at least one beacon will pass close enough to the asteroid to yield meaningful gravity measurements without impacting it. This lack of control introduces risk and reduces mission reliability.

By contrast, the second strategy, i.e., performing a controlled close flyby of the host spacecraft while using the beacons as free-space references, offers significant advantages. It eliminates the risk of losing probes due to collision, enables precise control of the flyby geometry through spacecraft autonomy, and focuses gravitational sensitivity where tracking is most accurate. This method decouples tracking geometry from close-proximity operations, increasing flexibility in deployment and mission design. Importantly, this approach is well within current technological capabilities, as demonstrated by autonomous targeting and navigation in missions such as Deep Impact [2], Rosetta [53], DART [16], Hayabusa and Hayabusa2 [56, 57], OSIRIS-REx [31], and Lucy [33].

In summary, the GIRO and APIC systems offer an unprecedented combination of high-accuracy Doppler and optical measurements, enabling robust mass estimation even during high-velocity flybys of small bodies.

4 Methods for Asteroid Mass Determination

In the context of planetary defense and physical characterization, the most effective method for accurately determining the mass of a small body is through in situ spacecraft tracking, either via rendezvous or close flyby. These approaches enable direct sensing of the gravitational influence exerted by the target on the spacecraft's trajectory, allowing estimation of its gravitational parameter (GM). Although less accurate than rendezvous, flybys represent a faster and more resource-efficient solution, particularly well suited for rapid reconnaissance missions targeting newly discovered potentially impacting asteroids. In such scenarios, where time is critical, a well-designed flyby can yield sufficient dynamical information for a reliable mass estimate. However, accurately determining the mass of small bodies remains challenging, as the achievable precision strongly depends on the quality of Doppler tracking data and the mission's ability to measure the subtle trajectory perturbations induced by the asteroid's weak gravitational field.

The primary gravitational interaction between the asteroid and the spacecraft manifests as a perturbation in the spacecraft's heliocentric velocity, denoted as ΔV. For this reason, high-precision Doppler tracking is essential to measuring the asteroid's mass signature on the spacecraft path. Figure 3 illustrates the hyperbolic flyby geometry.

The main goal is to measure the deflection angle φ, which quantifies the change in the spacecraft's velocity vector between the inbound and outbound asymptotes of the hyperbolic flyby, as a result of the asteroid's gravitational pull. The magnitude of

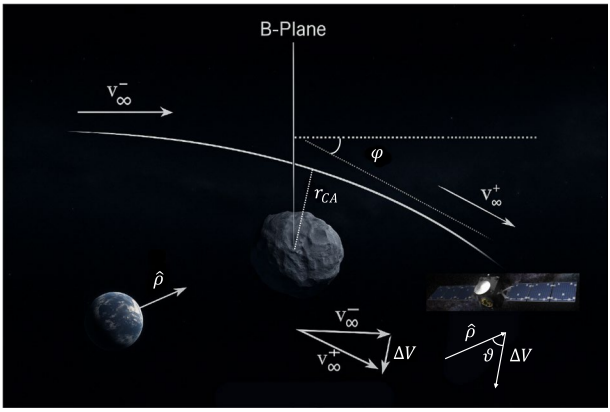

Fig. 3 Schematic of hyperbolic flyby geometry and velocity deflection

this deflection, and thus the corresponding velocity change ΔV, depends primarily on three factors: the asteroid's GM, the hyperbolic excess velocity V_∞, and the CA distance r_{CA} from the asteroid's center of mass. The expected velocity change can be approximated by [6]:

$$\Delta V = \frac{2GMV_\infty}{r_{\mathrm{CA}}V_\infty^2 + GM} \approx \frac{2GM}{r_{\mathrm{CA}}V_\infty}. \tag{1}$$

Doppler tracking, usually performed by Earth-based stations such as the DSN or ESTRACK, provides high-sensitivity measurements of velocity along the Earth-spacecraft line of sight direction. However, only the component of ΔV projected on this line contributes to the observed Doppler signal. Denoting the angle between ΔV and the line-of-sight unit vector $\hat{\rho}$ as ϑ (see Fig. 3), the observed component becomes:

$$\Delta V_{\mathrm{obs}} = \Delta V \cos\vartheta. \tag{2}$$

Combining Eqs. 2 and 1, an estimate of the asteroid's mass can be written as:

$$M = \frac{\Delta V_{\mathrm{obs}}\, r_{\mathrm{CA}}\, V_\infty}{2G} = \frac{\Delta V \cos\vartheta\, r_{\mathrm{CA}}\, V_\infty}{2G}. \tag{3}$$

In this formulation, the most controllable parameter is the flyby distance r_{CA}. The geometry angle ϑ is governed by the line-of-sight configuration, while V_∞ is set by orbital dynamics. These constraints highlight the importance of optimizing both close approach distance and Earth-view geometry in traditional Doppler-based flybys.

Furthermore, the formal uncertainty in the estimated GM can be approximated by differentiating Eq. 1, leading to:

$$\sigma_{GM} \approx \frac{1}{2} b V_\infty \sigma_{\Delta V}, \tag{4}$$

where b is the impact parameter (typically close to r_{CA} for weak deflections) [28], and $\sigma_{\Delta V}$ is the 1σ uncertainty in the measured velocity change.

Equation 4 is based on simplifying assumptions, neglecting uncertainties in the asteroid and spacecraft states as well as the flyby geometry. Nonetheless, it provides a first-order estimate of the expected uncertainty. Assuming typical Earth-based Doppler noise levels, on the order of 0.1 mm/s for X/X-band links and 0.01 mm/s for Ka/Ka, and 0.005 mm/s when using dual-link data in combination with a Water Vapor Radiometer (WVR) to mitigate plasma effects [10], and an optimal Earth geometry ($\vartheta \approx 0$), Eq. 4 suggests that the uncertainty in GM becomes prohibitively large for small bodies in standard flyby scenarios.

In this context, Table 1 presents the relative GM uncertainties derived from OD simulations assuming continuous DSN tracking over a ±7-day window around CA (see Sect. 6 for simulation details). The scenario assumes a bulk density of 1000 kg/m^3, with a flyby altitude of 50 m and a relative velocity of 5 km/s. The results show that, even under favorable Earth-viewing geometry, meaningful GM observability is achieved only when dual-link + WVR Doppler data are combined with APIC optical images, which are used to improve the host–asteroid relative navigation solution. Since GIRO optical images are not included in this analysis, the benefit of APIC comes entirely from the improved spacecraft–asteroid geometry determination; in the absence of imaging data, the a priori uncertainties in both the asteroid and spacecraft positions dominate the estimation error. In the combined configuration, the relative GM uncertainty is approximately 5% for a 600 m diameter asteroid, around 21% for a 300 m target, and becomes prohibitive for diameters below 300 m. As a result, due to the requirement for optimal Earth-based geometry and the poor performance for very small asteroids, this approach is deemed impractical for rapid-response planetary defense scenarios.

To overcome these limitations, as previously discussed, a promising solution involves the use of GIRO beacons. In a representative scenario, one or more beacons are deployed from the host spacecraft to enable precise position determination via triangulation in deep space during the flyby (see Fig. 4). The enhanced GIRO Doppler accuracy allows the detection of the target asteroid's weak gravitational signal with significantly improved precision, and eliminates the need for favorable Earth-spacecraft geometry.

For example, as depicted in Fig. 4, consider a GIRO on a trajectory aligned with both the host spacecraft and the direction of gravitational acceleration at CA. This configuration maximizes the Doppler information content near CA between the two elements. In this context, Doppler data acquired by GIRO within a short time window

Table 1 Estimated relative uncertainty on the gravitational parameter GM, computed numerically through OD simulations for asteroids of varying diameters. The scenario assumes a host-spacecraft only flyby at 50 m altitude above the surface with a relative velocity of 5 km/s, a bulk density of 1000 kg/m, and typical Earth-based Doppler tracking noise under optimal Earth-view geometry ($\vartheta \approx 0$)

Asteroid diameter	Link			
	X-X	Ka-Ka	Dual + WVR	Dual + WVR + APIC images
	(0.1 mm/s)	(0.01 mm/s)	(0.005 mm/s)	
300 m	Not observable	Not observable	Not observable	∼21%
600 m	Not observable	Not observable	Not observable	∼5%

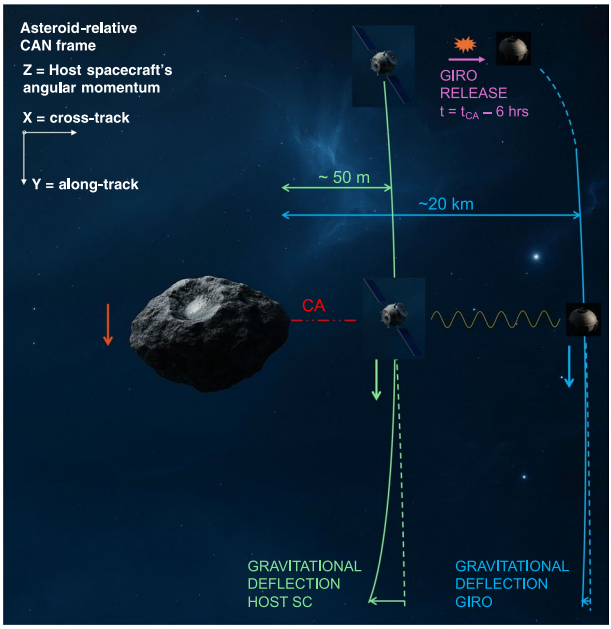

Fig. 4 Schematic representation of the GIRO flyby geometry showing unperturbed (dashed) and perturbed (solid) trajectories for the host spacecraft and GIRO beacon. The gravitational acceleration from the asteroid causes a measurable deflection, which is larger for the host due to its closer approach. The differential deflection between the two trajectories is the key observable used to estimate the asteroid's GM. The directions are expressed in an asteroid-relative Cross-track, Along-track, Normal (CAN) reference frame. After release, the GIRO receives a small ΔV, so its orbital angular momentum vector is not exactly identical to that of the host; however, given that the ΔV is very small compared to the flyby relative velocity, the two vectors remain nearly parallel. Spacecraft distances are not shown to scale

around CA yields a formal uncertainty in GM, derived from numerical OD simulations, that matches the analytical prediction of Eq. 4.

Nevertheless, it is important to note that in such scenarios, although the instantaneous gravitational deflection at CA is measurable, it is relatively modest for small bodies and thus contributes limited information by itself. However, this small deflection is sufficient to induce a slight divergence between the trajectories of the host spacecraft and the GIRO, which have experienced different gravitational accelerations. This differential deflection accumulates over time and becomes increasingly observable in the post-flyby phase (see Fig. 4). As a result, most of the information relevant to precise GM estimation is expected to come from continued tracking after the encounter. Our orbit determination simulations confirm that post-encounter data enable accurate GM recovery, even for very small NEAs. See Sect. 7 for quantitative results.

5 Flyby Concept of Operations

This work focuses on the critical phases immediately before and after the asteroid flyby, which are the most relevant for mass determination. Specifically, the analysis considers a symmetric two-week window around the CA, during which tracking data are acquired and processed. It is assumed that, prior to this window, the heliocentric trajectory of the spacecraft is determined at the km-level, as typically ensured by the navigation teams of deep-space missions.

No specific launch or encounter dates are assumed in this study, and a detailed mission design is not performed. The objective is to characterize the achievable mass estimation accuracy using GIRO in a way that is broadly applicable, independent of launch date, target geometry, or Earth-spacecraft configuration. As discussed earlier, GIRO enables accurate mass determination without reliance on Earth's position, since both the Doppler shift at CA and the differential deflection are observed directly in deep space. In addition, combined GIRO and APIC tracking allows for GM estimation based solely on relative measurements to the target. While Earth-based data are not required in principle, they remain useful for refining the asteroid's ephemeris. The asteroid 2024 YR4 is used as a reference case, but the methodology and findings are subsequently generalized to a range of asteroid sizes and densities.

The proposed concept of operations for this reconnaissance mission spans from one week before to one week after the asteroid encounter. During this period, optical images of the target are acquired to refine the spacecraft's relative position. Nominally, one image is captured every two hours. Throughout the entire pre- and post-flyby phase, the host spacecraft is continuously tracked by the DSN using Doppler measurements (60-second count time) and range measurements (300-second count time).

Between 6 and 12 h before the flyby, one or more GIROs are released from the host spacecraft in directions that ensure they remain at safe distances and serve as free space references during the flyby, without interfering with the close encounter. From the moment of release until one week after the flyby, the GIROs are continuously tracked via range-rate measurements (at 60 s count times) by the host spacecraft. After release, the GIROs are expected to be optically tracked to determine their spin states with a precision better than 0.1 μm/s in range-rate, and we assume in this work that this characterization has already been performed, resulting in a clean Doppler signal. In addition, GIRO optical images are not included in our analysis, as they do not provide information that is critical for the asteroid GM estimation.

Around two hours before closest approach, we assume that the spacecraft's autonomous navigation system takes over and executes a series of terminal guidance maneuvers to guarantee the desired flyby conditions. The specific onboard guidance logic is not simulated here, as such modeling lies beyond the scope of this study and its effectiveness has already been demonstrated by previous missions (e.g., Deep Impact, DART). Nevertheless, the execution uncertainties of these maneuvers are incorporated into our dynamical model, since they affect the flyby geometry and, consequently, the achievable GM accuracy. Further details are provided in Sect. 6.3.

During the most critical phase–between one hour before and one hour after CA–the image acquisition cadence increases to one image every 10 s. After this period,

the nominal schedule resumes, with one image taken every two hours. To remain conservative, this study excludes images acquired within CA± 1 min, as center-finding errors during that interval are expected to be dominated by uncertainties in the asteroid's shape rather than limitations in image processing. However, if the host spacecraft is equipped with an infrared camera, a joint post-flyby analysis of infrared and optical images could help reduce the overall image noise. As a result, these images could be included in the estimation filter to further improve the state and orbit determination of both the asteroid and the spacecraft. It is worth noting that the use of an APIC camera with internal pointing capability eliminates the need for any spacecraft slews entirely during the image data gap.

Figure 5 summarizes the concept of operations timeline for the GIRO asteroid flyby mission.

This comprehensive dataset, combining Earth-based radiometric tracking, optical navigation of the host spacecraft relative to the asteroid, and high-precision Doppler tracking of the GIROs, provides a robust foundation for accurately determining the mass of very small asteroids, including those in the 60 m diameter range such as 2024 YR4. In particular, knowledge of the inbound asymptote relative to the asteroid, provided by optical imaging, combined with the GIRO Doppler data at CA, and especially the differential deflection measurements captured via GIRO Doppler after the flyby, constitutes the core dataset driving the mass estimation process.

6 Simulation Setup

The OD simulations are carried out using NASA JPL's Mission Analysis, Operations, and Navigation Toolkit Environment (MONTE) [18, 36, 37]. The following sections describe the dynamical, measurement and maneuver models, and filter configuration used in the simulation.

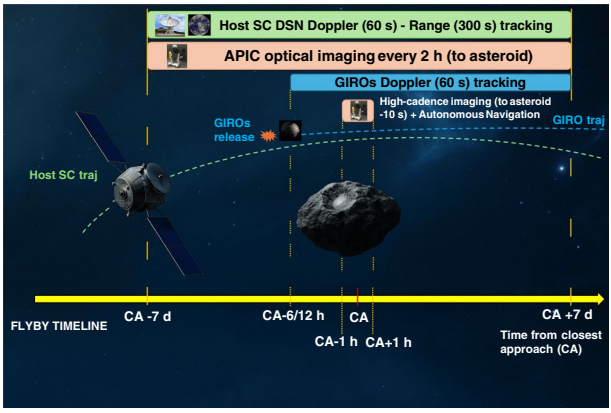

Fig. 5 Concept of operations timeline for the GIRO asteroid flyby mission. The figure illustrates continuous DSN radiometric tracking of the host spacecraft from seven days before the encounter to seven days after, GIRO deployment 6–12 h before CA and continuous Doppler tracking, APIC optical imaging of the asteroid every 2 h for the whole time-window, and high-cadence 10 s imaging during CA

6.1 Dynamical Model

The OD process requires accurate modeling of the relevant dynamical environments. In this study, we consider the heliocentric orbits of the 2024 YR4 asteroid and the host spacecraft, as well as the trajectories of the deployed GIRO beacons. The heliocentric orbital parameters of asteroid 2024 YR4 used in the simulation are listed in Table 2.

The gravitational forces considered in the simulation include the point-mass perturbations from the Sun, the Moon, the eight planets, and Pluto. The positions and velocities of these bodies are obtained from the DE441 planetary ephemerides [42]. Relativistic corrections due to the Sun, the Moon, and the planets are also included, using the Einstein–Infeld–Hoffman formulation [37]. In addition, the asteroid's force model accounts for gravitational perturbations from the 343 most massive main-belt asteroids and 30 individual Kuiper Belt Objects (KBOs) [42].

For the host spacecraft and GIROs, the force model also includes the gravitational acceleration due to the asteroid target. Non-Gravitational Accelerations (NGA) are modeled through Solar Radiation Pressure (SRP), which is computed using a host spacecraft's realistic shape model and a spherical shape for the GIROs. The total SRP force is calculated as the sum of contributions from individual components, each characterized by distinct geometry, surface properties, and orientation with respect to the Sun. In addition, to account for unmodeled non-gravitational forces, such as thermal re-radiation [40], asteroid thermal emission, and albedo effects, stochastic accelerations are applied to all spacecraft. These are intended to capture residual modeling errors, particularly during the flyby phase. A batch time of 8 h is assumed, with a stochastic acceleration magnitude of 10^{-12} $\mathrm{km/s^2}$ applied to the host spacecraft, and 10^{-13} $\mathrm{km/s^2}$ to each GIRO unit [50].

6.2 Measurement Model

As previously described, the dataset combines Earth-based radiometric measurements, inter-satellite (host-to-GIROs) range-rate data, and optical images of the target asteroid.

Earth-based Doppler measurements are modeled with a noise level of 0.1 mm/s (over 60 s count times), while range data include a 1-meter uncertainty. A range bias is also estimated for each pass, with an a priori uncertainty of 15 m.

For GIRO range-rate measurements, [45] reported an expected accuracy between 0.1 and 0.5 $\mu\mathrm{m/s}$. In this study, we consider three Doppler noise scenarios: a require-

Table 2 2024 YR4 asteroid orbital parameters from JPL solution 78 [38]

Parameter	Value
Semimajor axis	2.516 au
Orbital period	3.991 years
Eccentricity	0.662 deg
Inclination (EMO2000)	3.408 deg
Diameter	60 ± 7 m [48]
Pole direction (ecliptic longitude, latitude)	$\lambda, \beta = 42, -25$ deg [9]

ment-level noise of $1\ \mu\mathrm{m/s}$, an expected performance of $0.1\ \mu\mathrm{m/s}$, and a test case based on GRAIL-level accuracy of $0.01\ \mu\mathrm{m/s}$, all assuming 60 s count times. We analyze all three scenarios, but the baseline for the nominal results in Sect. 7 adopts the $0.1\ \mu\mathrm{m/s}$ scenario. Further details on the GIRO noise budget and signal characteristics can be found in [45].

Optical imaging of the asteroid is assumed to be conducted using the APIC camera system onboard the host spacecraft [46]. For each image, a measurement noise of 0.5 pixels (in both sample and line) is assumed, along with an estimated pointing error per image with a 2 arcsecond a priori uncertainty [46].

Table 3 summarizes the assumed noises in this work.

6.3 Maneuver Model

In addition to the stochastic accelerations described in Sect. 6.1, the dynamical model incorporates the uncertainties associated with the impulsive maneuvers that occur during the mission timeline. We consider two classes of maneuvers: (i) the GIRO release maneuvers, and (ii) the terminal guidance maneuvers executed by the host spacecraft to ensure the targeted close flyby.

6.3.1 GIRO Release Maneuvers

Each GIRO beacon is deployed through a controlled release that imparts a ΔV of approximately 1 m/s to the probe. To avoid double-counting the same dynamical event, only the reaction ΔV acting on the host spacecraft is estimated in the filter, while the equal-magnitude and opposite-direction ΔV applied to the beacons is not independently estimated. The maneuver components are defined in the asteroid-relative CAN frame, and an a priori 1σ uncertainty corresponding to 5% of the nominal 1 m/s release ΔV is assigned to each component. These uncertainties allow the OD filter to capture the small but non-negligible perturbations introduced by the deployment events.

6.3.2 Terminal Guidance Maneuvers

In the baseline mission concept, the final targeting of the host spacecraft is performed autonomously during the last few hours before CA. The detailed onboard guidance

Table 3 Summary of the measurement uncertainties adopted in the OD simulations (1σ)

Earth-based tracking	GIRO tracking	Optical-APIC camera
Doppler: 0.1 mm/s at 60 s integration time	Doppler: 1 $\mu m/s$ (requirement), 0.1 $\mu m/s$ (expected performance), and 0.01 $\mu\mathrm{m/s}$ (test case using GRAIL accuracy) at 60 s integration time	Sample / Line accuracy: 0.5 pixels
Range: 1.0 m (one measurement every 300 s) Range Bias: 15 m on each tracking passage (estimated)		Spacecraft attitude: 2 arcsec (from APIC - [46])

and execution algorithm is not modeled in this work, as its implementation is out of scope. Moreover, past missions (e.g., Deep Impact AutoNav, DART SmartNav) have already demonstrated the feasibility of accurate high-velocity terminal navigation. However, the uncertainties associated with these maneuvers must be included, as they influence the geometry of the flyby and therefore the quality of the GM estimation.

Based on the maneuver timelines of previous missions, we assume that the terminal guidance sequence consists of four impulsive maneuvers, executed at [7, 20]:

- CA - 2 h;
- CA - 80 min;
- CA - 50 min;
- CA - 20 min.

The maneuver vectors are defined again in the asteroid-relative CAN frame. Following Mastrodemos et al. [35], maneuver execution errors for burns of order 1–7 m/s are typically within 4–10 cm/s, corresponding to 1–5% of the total ΔV. DART SmartNav and Deep Impact AutoNav operations reported ΔVs below 3 m/s. Accordingly, we adopt a conservative 1σ uncertainty of 3.5 cm/s per component for each autonomous maneuver. This magnitude corresponds to a total ΔV uncertainty of approximately 6 cm/s per maneuver when combining the three directional components.

6.3.3 Tracking Data During the Autonomous Navigation Window

All radiometric and optical tracking data acquired during the terminal guidance window are retained in the OD filter. Since the detailed auto-navigation algorithm is not explicitly simulated, these data provide the necessary constraints to reconstruct the spacecraft state before and after each maneuver while the maneuver execution uncertainties capture the dynamical discontinuities.

This approach ensures a realistic representation of the mass estimation performance without requiring a full simulation of the onboard guidance algorithm. The final maneuver executed at CA-20 min is expected to reduce the B-plane uncertainty to the level required to safely achieve a 50 m flyby, consistent with demonstrated heritage from previous missions.

6.3.4 Sensitivity to the Timing of the Final Maneuver

To assess the robustness of the mass determination to uncertainties in the terminal guidance timeline, Sect. 7.3 presents a sensitivity analysis in which the execution time of the final autonomous maneuver is varied. The resulting variation in the GM uncertainty quantifies how late-execution navigation updates affect the ability to recover the asteroid mass.

6.4 Filter Setup

The primary objective of the sensitivity analyses in this study is to assess the formal uncertainties associated with the asteroid's GM estimation during a flyby mission

employing GIRO beacons. The estimated parameters include the asteroid's GM, the state vectors of the asteroid, the host spacecraft and GIROs, host spacecraft SRP scale factor, pointing bias per image, and range bias per tracking pass.

A complete summary of the estimated parameters and their associated a priori uncertainties is provided in Table 4.

7 Results

This section presents the results of the GIRO-based OD simulations, focused on estimating the mass of asteroid 2024 YR4 during a close flyby, assuming a Bennu-like density of 1190 kg/m^3. The baseline scenario assumes a flyby at 50 m altitude above the asteroid's surface (i.e. about 80 m with respect to the center of the asteroid) and 5 km/s relative velocity. The analysis is then extended in the following subsections to explore the sensitivity of the mass estimate to various mission parameters, includ-

Table 4 Filter setup for the OD simulations. The 2024 YR4 GM is provided as reference, assuming a Bennu-like density of 1190 kg/m^3, the 1000% apriori uncertainty is considered also for the other range of asteroid sizes and densities analyzed in Sect. 7.4

Parameter	A priori 1σ	Notes
Host Spacecraft State		
Position	1 km	Host SC state estimated with respect to the Sun
Velocity	1.0 m/s	
GIROs Beacon State		
Position	1 m	GIROs state estimated with respect to the Host SC
Velocity	0.1 m/s	
2024 YR4 State		
Position	10 km	2024 YR4 with respect to the Sun. Widely open
Velocity	1.0 cm/s	
2024 YR4 GM	$8.98 \cdot 10^{-11}$km^3/s^2	1000%. Widely open
Solar Radiation Pressure		
Scale factor Host SC	1.0	100% of the acceleration
Maneuvers		
GIROs release (DX-DY-DZ)	5.0 cm/s	Uncertainty of each component, defined in the asteroid-relative CAN frame, corresponding to 5% of the releaseΔV
4 Terminal guidance maneuvers (DX-DY-DZ)	3.5 cm/s	Uncertainty of each component, defined in the asteroid-relative CAN frame
Stochastic Accelerations		
Host SC	10^{-12}km/s^2	Set of 3 stochastic accelerations (X-Y-Z) estimated in uncorrelated batches of 8 h
GIROs	10^{-13}km/s^2	Set of 3 stochastic accelerations (X-Y-Z) estimated in uncorrelated batches of 8 h
Pointing Error Per Picture		
APIC 3 rotations	2 arcsec	From APIC [46]
DSN Range Bias Per Pass	15 m	

ing the number of GIROs, asteroid size and density, flyby distance and velocity, and measurement noise levels. The OD setup and measurements adopted herein are the ones described in Sects. 5–6.

7.1 Sensitivity to beacon release geometry

This subsection investigates how the release geometry, specifically, the direction and number of deployed GIRO beacons, affects the accuracy of the recovered asteroid mass. We begin by analyzing the sensitivity of the mass determination to the release direction of a single beacon, using the baseline scenario, 50 m flyby altitude of the host spacecraft relative to asteroid 2024 YR4, with a flyby velocity of 5 km/s, and GIRO expected performance Doppler noise. The analysis is then extended to two- and three-beacon configurations to identify combinations of release vectors that provide favorable tracking geometries and minimize the formal uncertainty on the asteroid's GM.

To perform this assessment, a parametric study was conducted by sampling a wide range of possible release directions. These directions were generated using a Fibonacci lattice, which yields a quasi-uniform distribution of unit vectors over the surface of a sphere. Each direction corresponds to an impulsive release maneuver of 1 m/s applied to the beacon at the time of deployment (assumed to be 6 h before CA).

The release vectors are defined in an asteroid-relative Cross-track, Along-track, and Normal (CAN) reference frame at the time of release (see Fig. 4). Specifically, the host spacecraft's velocity relative to the asteroid defines the Y-axis (along-track). The Z-axis is aligned with the host spacecraft's angular momentum vector relative to the asteroid, and the X-axis is defined as the cross product of the Y- and Z-axes, corresponding to the cross-track direction.

For each release direction, a full OD simulation was performed using MONTE, incorporating all data and models described in Sects. 5-6. The formal uncertainty on the asteroid's GM was computed through covariance analysis. In total, 500 unique release configurations were evaluated, and the resulting σ_{GM} values were mapped as a function of the release direction. This analysis enabled the identification of geometries that maximize sensitivity to gravitational deflection and minimize the uncertainty in the mass estimate.

Figure 6 shows the retrieved formal 1σ uncertainty on GM as a function of release orientation at the time of ejection. Notably, the best results are obtained when the beacons are released along the cross-track directions (±X), with the outcomes being symmetrical, as expected. Given the flyby geometry and frame, releasing the beacon along +X places it beside the host spacecraft at CA, resulting in a near-alignment of the host, beacon, and asteroid, see Fig. 4. As can be seen, this configuration offers several advantages:

- The GIRO Doppler signal is well-aligned with the gravitational acceleration vector at CA, maximizing sensitivity to the asteroid's gravity along the line of sight.
- The beacon passes significantly farther from the asteroid (approximately 20 km along +X for a release 6 h before CA), while the host spacecraft performs a close flyby at roughly 50 m.

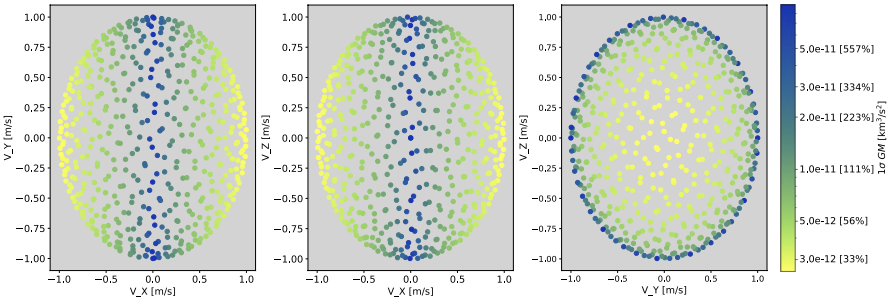

Fig. 6 3D visualization of the formal uncertainty on the asteroid GM as a function of the beacon release direction, using a single GIRO. Each point represents a simulated GIRO release geometry with a 1 m/s impulse burn in a specific direction, and is colored according to the corresponding σ_{GM} value obtained from the OD simulation. The directions are expressed in an asteroid-relative CAN reference frame at the time of release. The simulations assume the baseline flyby scenario of 50 m altitude above the surface, relative velocity of 5 km/s, and GIRO Doppler noise of $0.1\ \mu\mathrm{m/s}$

As a result, the beacon experiences a weaker gravitational perturbation, leading to a larger differential deflection between the host and beacon trajectories after the flyby (see Fig. 4). This enhanced separation improves the observability of the differential acceleration projected along the line of sight between the two elements, enabling more informative Doppler measurements and thus reducing the formal uncertainty on the asteroid's mass.

Figure 6 shows that releasing the GIRO in the flyby plane in the cross-track direction yields the lowest formal uncertainties, reaching values as low as $2.6 \cdot 10^{-12}\ \mathrm{km}^3/\mathrm{s}^2$, which corresponds to a relative error of approximately 29% for 2024 YR4 with a Bennu-like density and baseline flyby scenario.

Importantly, even when accounting for realistic release errors, such as a 5% uncertainty in the cross-track component of the beacon's release velocity, the resulting mass uncertainties remain comparable, as shown in Fig. 6. This indicates that small deviations from the optimal release direction do not significantly degrade estimation performance.

Conversely, Fig. 6 shows that releasing the beacon in the along-track direction (i.e., Y-axis, ahead of or behind the host spacecraft), or along the ±Z direction, leads to a significant loss of GM observability. In the along-track direction release, both the host and beacon pass the asteroid at nearly the same distance and time, experiencing similar gravitational accelerations. As a result, their post-flyby trajectories diverge only slightly, producing a minimal differential deflection. This, in turn, introduces strong correlations between the estimated GM and the initial velocity states of both the spacecraft and the asteroid, rendering the estimation problem ill-conditioned and significantly increasing the formal uncertainty, up to $8 \cdot 10^{-11}\ \mathrm{km}^3/\mathrm{s}^2$, making GM effectively unobservable for 2024 YR4. To conclude, as shown in Fig. 6, this analysis highlights the importance of having a non-zero release component along the cross-track direction in order to enable a meaningful estimation of the asteroid's GM.

This analysis is then extended to scenarios involving two GIROs. While very good performance is already achieved using a single GIRO, we foresee and recommend the deployment of at least two GIROs per flyby to provide redundancy and ensure

mission robustness. To simplify the analysis, and given the demonstrated benefits of releasing a beacon on the cross-track direction, we fix the release direction of GIRO-1 along +X. A new Monte Carlo analysis is then performed to determine the optimal release direction for GIRO-2, which is assumed to be ejected 5 min after GIRO-1.

Figure 7 shows the resulting formal 1σ uncertainty on GM as a function of the release direction of GIRO-2. In the best release condition, adding a second GIRO decreases the uncertainty by a factor of 1.4 compared to the single-GIRO scenario, from 29% down to 20% relative uncertainty. As in the one-GIRO case, the lowest uncertainties are achieved when GIRO-2 is released near the cross-track direction (±X), which provide favorable geometry at CA and maximize differential deflection after the flyby. Nevertheless, releasing GIRO-2 at an intermediate angle (e.g., 45 deg between -Y and ±X) is recommended to avoid potential geometric conflicts between the beacons, even if they are released at different times.

It is worth noting that testing alternative configurations for GIRO-1 (combined with new Monte Carlo simulations for GIRO-2) did not yield better results; the best performance is consistently obtained when GIRO-1 is released cross-track.

To conclude, assuming GIRO-1 is released along +X and GIRO-2 at 45 deg between -Y and +X, introducing a third beacon provides an additional improvement of approximately a factor of 1.3 relative to the two-beacon configuration, with the best relative uncertainties-when GIRO-3 is released along the cross-track direction (-X) -on the order of 18%. For brevity, the detailed analysis of the optimal GIRO-3 release direction is not included here. A third GIRO also provides valuable redundancy.

7.2 2024 YR4 Mass Estimation Performance

Building on the previous analysis of the relationship between release direction, flyby geometry, and dynamical estimation accuracy, we adopt the best-case release configuration, with GIRO-1 deployed along the cross-track (+X) direction. In the two- and three-GIRO simulations, GIRO-2 is assumed to be released at $45°$ between the -Y

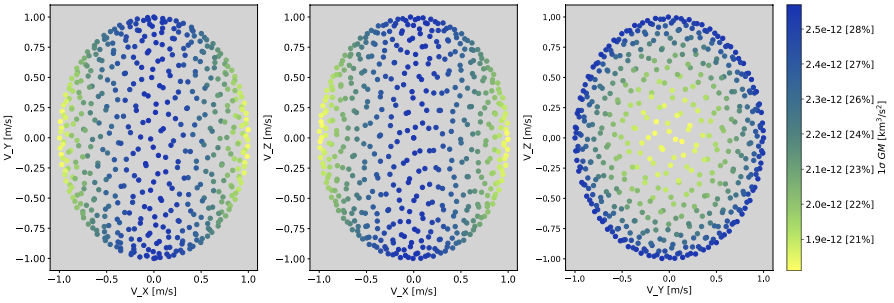

Fig. 7 3D visualization of the formal uncertainty on the asteroid GM using two GIROs, as a function of the GIRO-2 release direction, with GIRO-1 fixed along the +X direction (the optimal case, see Fig. 6). Each point represents a simulated GIRO-2 release geometry, based on a 1 m/s impulse in a specific direction, and is color-coded according to the corresponding σ_{GM} value obtained from the orbit determination simulation. The directions are expressed in an asteroid-relative CAN reference frame at the time of release. The simulations assume the baseline flyby scenario of 50 m altitude above the surface, relative velocity of 5 km/s, and GIRO Doppler noise of $0.1\ \mu\mathrm{m/s}$

and +X directions behind the host spacecraft, enhancing triangulation while avoiding potential trajectory conflicts between the beacons, whereas GIRO-3 is ejected along the cross-track (-X) direction.

The flyby altitude is fixed at 50 m, and the relative velocity at 5 km/s. The GM of 2024 YR4 is again computed assuming a Bennu-like bulk density of 1190 $\mathrm{kg/m^3}$ and a radius of 30 m, yielding a reference value of $8.98 \cdot 10^{-12}$ $\mathrm{km^3/s^2}$. To remain conservative, as mentioned in Sect. 5, no images acquired within ±1 min of CA are included in the filter.

Table 5 summarizes the OD nominal results obtained using the reference stochastic accelerations (see Table 4) for various flyby configurations, varying the number of deployed GIROs. As shown, the host spacecraft alone does not provide sufficient observability of the asteroid's GM, even under favorable Earth-flyby geometry assumptions and adopting a dual-link Doppler data together with the WVR calibration. Adding the beacons using the GIRO requirement Doppler accuracy still does not allow observability for flybys at 5 km/s or faster. However, a substantial improvement is achieved if using the expected Doppler performance level (0.1 $\mu\mathrm{m/s}$), in which case a single GIRO can estimate the GM with a relative uncertainty of 29%, which improves to 3% if considering typical GRAIL accuracies (0.01 $\mu\mathrm{m/s}$). As expected, the formal uncertainty on GM scales approximately linearly with the GIRO Doppler accuracy.

Moreover, as demonstrated earlier, the results indicate that adding a second or third GIRO beacon yields good improvements in GM estimation, about a factor of $1.6-1.7$ when increasing from one to three beacons, for both the expected GIRO performance and GRAIL-level accuracy. Under the expected Doppler accuracy, this translates to a GM relative uncertainty of approximately 23% and 18% when using a two- and three-beacon configuration, respectively.

It is also worth noting that the GIRO experiment estimates the asteroid's mass using purely relative measurements, making the GM determination independent of Earth-based tracking data. However, Earth-based observations remain important for constraining the asteroid's ephemeris.

Table 5 Formal 1σ uncertainties on the 2024 YR4 GM (reference value $8.98 \cdot 10^{-12}$ $\mathrm{km^3/s^2}$), obtained from simulated flybys at a fixed CA distance of 50 m above the asteroid's surface and a relative velocity of 5 km/s. Results are shown as a function of the number of deployed GIRO beacons (0 to 3) and for three GIRO Doppler noise levels. Relative uncertainties are shown in brackets

Configuration	$1\sigma_{GM}[\mathrm{km^3/s^2}]$ (GIRO acc. = 1.0μm/s)	$1\sigma_{GM}[\mathrm{km^3/s^2}]$ (GIRO acc. = 0.1μm/s)	$1\sigma_{GM}[\mathrm{km^3/s^2}]$ (GRAIL acc. = 0.01μm/s)
HostSC only	$9.0 \cdot 10^{-11}$ [not observable]	/	/
HostSC + 1 GIRO	$2.4 \cdot 10^{-11}$ [not observable]	$2.6 \cdot 10^{-12}$ [29%]	$3.2 \cdot 10^{-13}$ [3.6%]
HostSC + 2 GIRO	$2.0 \cdot 10^{-11}$ [not observable]	$2.1 \cdot 10^{-12}$ [23%]	$2.6 \cdot 10^{-13}$ [2.9%]
HostSC + 3 GIRO	$1.6 \cdot 10^{-11}$ [not observable]	$1.6 \cdot 10^{-12}$ [18%]	$1.9 \cdot 10^{-13}$ [2.1%]

Furthermore, an additional test was performed by increasing the magnitude of the stochastic accelerations up to 10^{-10} km/s^2 for both the host spacecraft and the beacons. Although these results are not reported in Table 5, they showed only a minor degradation–about 4 percentage points increase in relative uncertainty–with respect to the nominal case. As discussed in Sect. 3, the GIRO's spinner design, combined with a spin axis oriented normal to the host–GIRO velocity direction and the simultaneous deployment of multiple units are expected to largely suppress non-gravitational effects such as thermal re-radiation. Therefore, the tested value of 10^{-10} km/s^2 should be regarded as a conservative upper bound for the GIROs, and actual perturbations are expected to be significantly smaller.

Figure 8 shows the 1σ uncertainty in the asteroid's GM throughout the encounter (same flyby configuration as in Table 5, with 2 GIROs and 0.1 μm/s Doppler noise), plotted as a function of data accumulation in the filter. For this plot, 1-second integration time GIRO Doppler data is used to produce a smoother and more continuous curve around CA (with the 1 s data weighted as $\sigma_{1s} = \sqrt{60}\ \sigma_{60s}$).

As expected, the uncertainty remains nearly constant prior to CA, consistent with the a priori uncertainty, then drops sharply at CA when the GIRO Doppler tracking begins to provide information on the gravitational acceleration acting on the host spacecraft and the resulting differential trajectory deflection. Notably, about thirty minutes after CA, the GM accuracy has already improved to around 32%, and the uncertainty continues to decrease, reaching a plateau 6 h later at a 1σ relative uncertainty of 23%.

Figure 9 shows the evolution of the B-plane 3σ position uncertainty of the host spacecraft and the GIRO relative to the asteroid, expressed in the B R, B T, and Linearized Time of Flight (LTOF) components. The B-plane, widely adopted in the navigation community, is defined as the plane perpendicular to the incoming asymptote of the flyby trajectory and passing through the center of the target body [28, 52]. The projected position knowledge at CA improves progressively as more data are collected, with a sharp reduction at CA thanks to the GIRO Doppler tracking. Using post-flyby data, the reconstructed 3σ uncertainties for the host spacecraft are approximately 3.6 m in both the B R and B T components, and 4.2 s in LTOF. For the GIRO, the corresponding uncertainties are about 557 m in B R, 34 m in B T, and 4.2 s in

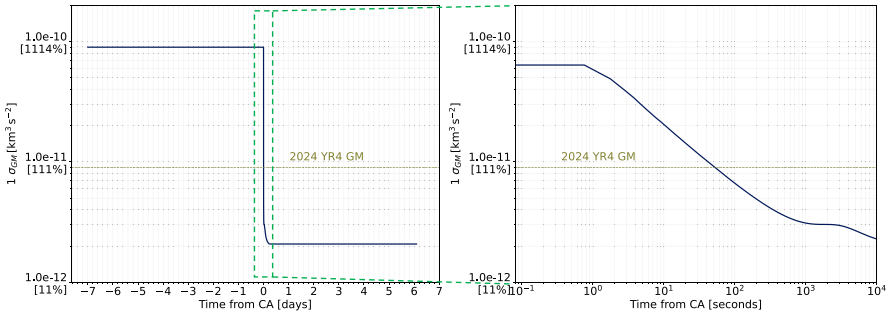

Fig. 8 Formal 1σ uncertainty on the 2024 YR4 GM as a function of time from CA, for a flyby with 2 GIROs and 0.1 μm/s Doppler noise. The host spacecraft performs the flyby at 50 m altitude above the asteroid's surface and 5 km/s relative velocity. The information gain begins at CA and plateaus 6 h later

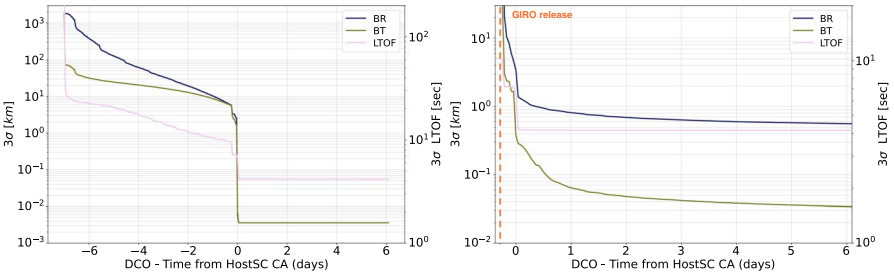

Fig. 9 B-plane 3σ formal uncertainty evolution of the host spacecraft (left panel) and GIRO-1 beacon (right panel) with respect to 2024 YR4, between CA±7 days. The B-plane uncertainties are computed without modeling the onboard autonomous navigation algorithm; only the associated maneuver execution uncertainties are included. The resulting pre-flyby uncertainties reflect the reconstructed trajectory in the absence of active terminal guidance. In flight, autonomous navigation would reduce the B-plane uncertainty to the level required for the close flyby

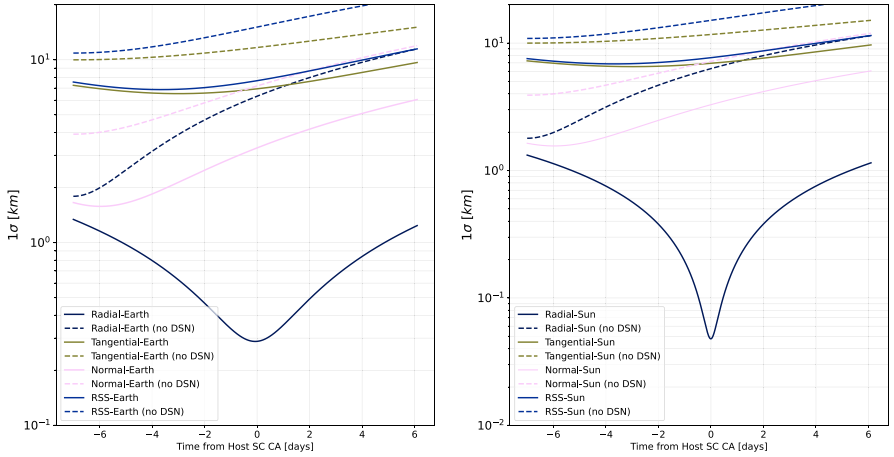

Fig. 10 Formal 1σ ephemeris uncertainty of 2024 YR4 with respect to the Earth (left panel) and Sun (right panel), expressed in the respective RTN frame

LTOF. The high uncertainty in LTOF is solely due to the exclusion of CA images from the estimation filter. This uncertainty can be significantly reduced by including those images in the analysis.

Furthermore, Fig. 10 shows the 1σ ephemeris uncertainty of 2024 YR4 relative to both Earth and the Sun, with and without Earth-based data. Looking at the reference scenario (with DSN data), even with a single flyby, the asteroid's radial position can be determined with an accuracy of approximately 300 m relative to Earth and 50 m relative to the Sun. The tangential and normal components remain at the kilometer level, as no images taken within ± 1 minute of CA are included in the filter. However, the radial and tangential components can be significantly reduced if images acquired at CA are processed and incorporated in filter. As mentioned earlier, although they are not directly relevant for the GM estimation, Earth-based observations remain essential for constraining the asteroid's ephemeris. Without these measurements, a

noticeable degradation appears in all state components of Fig. 10, with the radial component worsening by more than one order of magnitude.

Finally, it is worth noting that: (i) the reported ephemeris uncertainty components relative to Earth and the Sun will vary for each flyby depending on the spacecraft's position relative to these bodies, and (ii) while the CA images help refine the orbits of both the spacecraft and the asteroid, they do not contribute to further improvements in the GM estimation.

Finally, Fig. 11 summarizes the key results for a two-GIRO configuration, considering different host spacecraft flyby distances (50 m, 100 m, 200 m, 500 m, and 1 km) and relative velocities (1 km/s, 5 km/s, and 10 km/s) with respect to 2024 YR4, assuming a Bennu-like density. For each case, OD simulations are run using both the GIRO Doppler requirement noise level (1.0 μm/s, shown as dashed lines) and the expected performance (0.1 μm/s, solid lines).

As expected, the 1σ formal uncertainty in GM increases linearly with flyby altitude, relative velocity, and Doppler noise. For the expected performance level, and considering the 1 km/s cases, the relative GM uncertainty remains below 25% for flybys at altitudes below 400 m, increasing to approximately 30% and 60% at 500 m and 1 km, respectively. This low-velocity regime yields the best results, with the optimal case–a 50 m flyby at 1 km/s with 0.1 μm/s Doppler noise–reaching a relative GM uncertainty below 5%. This scenario highlights the full potential of the GIRO concept for precise mass estimation of small bodies.

At higher velocities, the performance gradually degrades. For instance, at 5 km/s, a 50 m flyby yields an uncertainty of about 23%, increasing to 38% at 100 m and becoming prohibitive above 200 m. At 10 km/s, even a 50 m flyby results in 47% uncertainty, already limiting the reliability of the mass estimate, which becomes unfeasible at greater altitudes. However, adding a third GIRO in these fast?flyby scenarios further reduces the uncertainty, reaching values as low as 36% for a 50 m-10 km/s flyby (not shown in Fig. 11).

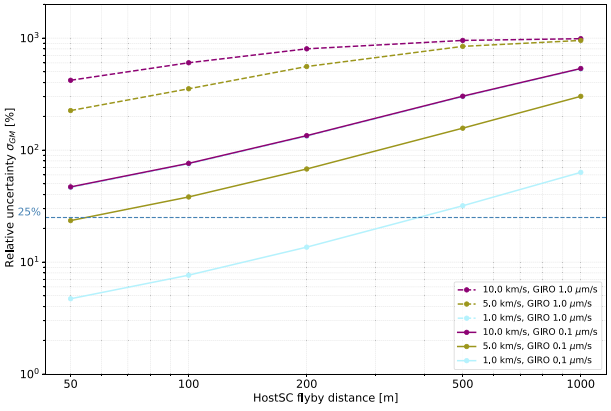

Fig. 11 Formal 1σ uncertainty on the 2024 YR4 GM as a function of flyby geometry and GIRO Doppler noise level. Solid lines indicate the expected GIRO Doppler performance (0.1 μm/s), while dashed lines show the requirement level (1.0 μm/s). Results refer to a configuration with two deployed GIROs, targeting 2024 YR4 with a Bennu-like density

Under the GIRO requirement noise assumption, the achievable performance is very limited. In this case, the best scenario– a 50 m flyby at 1 km/s– yields an uncertainty of approximately 47%, equivalent to the 10 km/s, 50 m, 0.1 $\mu m/s$ case, as expected, and already at the limit of a reliable mass estimate for a low-density, 60 m-diameter asteroid.

These results demonstrate the effectiveness of the GIRO concept in delivering precise gravity measurements and significant performance improvements across a broad range of encounter geometries and velocities, including rapid flybys of very small NEAs like 2024 YR4.

7.3 Flyby data information content

To assess how information content varies over time, we analyze the contribution of data acquired before, during, and after CA. This analysis informs the design and operations of planetary defense missions targeting PHAs or potentially impacting asteroids, particularly the robustness of mass estimation when the spacecraft performs autonomous maneuvers or rapid attitude slews near CA, such as those for terminal guidance or high-resolution imaging, which may alter NGAs (e.g., via SRP-induced mismodeling). Notably, such slews can be avoided if an APIC camera is used with a spacecraft fixed inertial orientation, thanks to its internal pointing capabilities. These results clarify whether such activities can be performed without compromising scientific return, or if a more disturbance-free trajectory is needed to ensure accurate mass estimation. The flyby geometry remains fixed at 50 m altitude above the surface and 5 km/s, and adopting two GIROs with expected performance noise.

Similarly to Fig. 8and 12 shows the results of OD simulations in which all GIRO data between CA–5 min and CA+30 min are excluded. As expected, in the absence of data

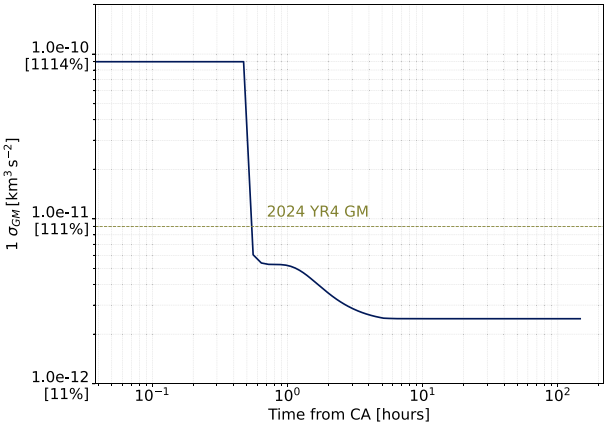

Fig. 12 Formal 1σ uncertainty on the 2024 YR4 GM as a function of time from CA, for a flyby with 2 GIROs and 0.1 μm/s Doppler noise, in which all GIRO data between CA-5 min and CA+30 min are excluded. The host spacecraft performs the flyby at 50 m of altitude and 5 km/s relative velocity. The information gain here begins at CA+30 min when GIRO tracking resumes, and plateaus approximately 6 h later

near CA, the GM uncertainty remains high until tracking resumes 30 min after CA, after which it drops sharply as post-flyby data is accumulated.

Remarkably, even without data around CA, a 1σ relative uncertainty of approximately 27% is still achieved, with only a 4 percentage points degradation in overall estimation performance. This confirms that the dominant contribution to GM recovery arises from the post-flyby differential trajectory deflection between the host spacecraft and the GIROs, provided that sufficient pre-flyby data is available to constrain the inbound asymptote. These findings highlight that, in the absence of major disturbances during the blind period, the key sensitivity for mass estimation lies in the post-flyby differential acceleration. While data around CA enhances the solution, high-accuracy estimation remains feasible even with limited availability during this critical phase.

Furthermore, all previous results assumed that the final terminal guidance maneuver is executed at CA–20 min. To assess the sensitivity of the GM estimation to the timing of this maneuver, Fig. 13 presents a complementary analysis in which the final burn epoch is varied from CA–30 min to CA–5 min, assuming the baseline flyby scenario and the expected GIRO Doppler performance. As shown, the formal GM uncertainty remains between 20–25% when the final maneuver is performed between 30 and 17 min before CA. As expected, the uncertainty increases as the maneuver is moved closer to CA, reaching 31% for a maneuver at CA–10 min and 44% at CA–5 min.

The final analysis examines the spacecraft's attitude behavior during the flyby. As previously discussed, the use of an APIC camera allows the spacecraft to maintain an inertially fixed attitude throughout the encounter. However, to provide guidance applicable to a wider range of planetary defense missions, this study investigates whether maintaining a fixed attitude and minimizing onboard activity during this critical phase is essential for reliable mass estimation.

To simulate the impact of different levels of onboard activity, we vary the stochastic acceleration batch time of the host spacecraft within a ±5-minute window centered on

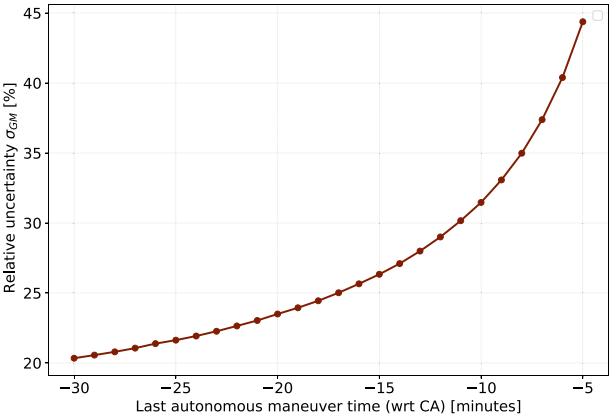

Fig. 13 Impact of the final terminal guidance maneuver execution time on the formal GM estimation uncertainty. The x-axis represents the assumed execution time of the last autonomous maneuver, varied to simulate different possible timing scenarios

Table 6 Estimated 1σ formal uncertainty in GM as a function of the stochastic-acceleration batch time applied to the host spacecraft within a ±5-minute window around CA, used to simulate different levels of onboard activity. Relative uncertainties are shown in brackets

Flyby scenario	$1\sigma_{GM}$ [km^3/s^2] - 5 min stochastics	$1\sigma_{GM}$ [km^3/s^2] - 1 min stochastics
50 m - 1 km/s	$2.1 \cdot 10^{-12}$ [23%]	$3.8 \cdot 10^{-12}$ [42%]
50 m - 5 km/s	$1.1 \cdot 10^{-11}$ [not obs.]	$1.9 \cdot 10^{-11}$ [not obs.]

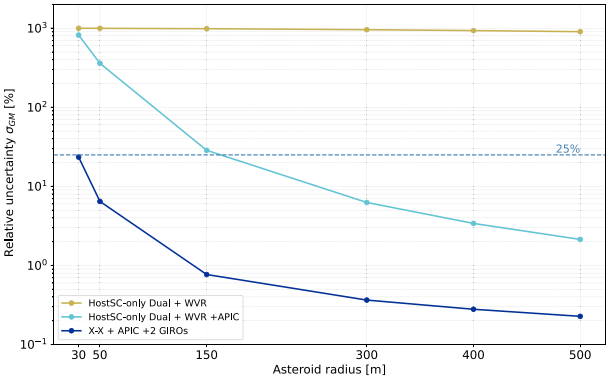

Fig. 14 1σ formal uncertainty in the asteroid's GM as a function of asteroid radius, assuming a Bennu-like bulk density of 1.19 g/cm^3, and the baseline flyby scenario of 50 m altitude above the surface at 5 km/s. The plot compares different flyby experiment configurations

CA. Specifically, two batch durations are tested: 5 min and 1 min. Outside this window, the batch time is kept constant at the nominal value of 8 h.

The OD results reported in Table 6 show that, for flybys of 2024 YR4 faster than 5 km/s, the GM estimation fails when using 5- or 1-minute batch durations. This highlights the critical importance of minimizing onboard activity within ±5 min of CA for fast flybys, to reduce the impact of unmodeled NGAs and to ensure a reliable mass determination. It also further underscores the benefits of adopting an APIC camera, which enables the spacecraft to avoid such rapid slews during the encounter.

7.4 Sensitivity to asteroid size and density

Finally, we present the results obtained by varying asteroid sizes and densities across different flyby configurations, to extend the analysis to a broader range of mission scenarios and targets. The flyby geometry assumes a 50 m altitude above the surface and a relative velocity of 5 km/s with respect to the asteroid.

Figure 14 illustrates the results for several configurations, assuming again a Bennu-like bulk density of 1.19 g/cm^3. First, we consider the host spacecraft alone under optimal Earth-based geometry ($\vartheta \approx 0$, see Fig. 3), assuming dual-link + WVR Doppler data. We then include the contribution of APIC optical images, which improve the spacecraft's relative position knowledge with respect to the asteroid. Finally, we examine the reference GIRO configuration with X-X Earth-based link, APIC images, and the addition of two beacons.

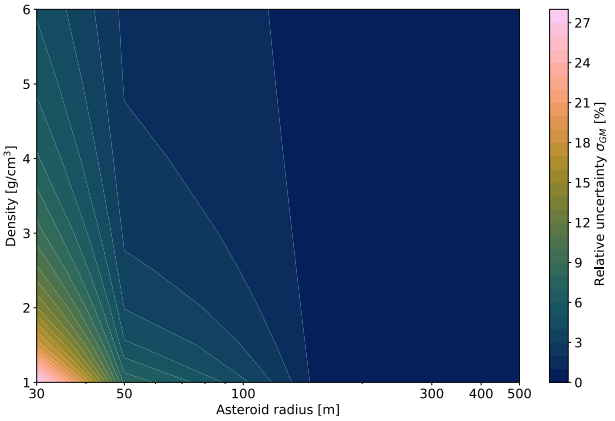

Fig. 15 Contour plot of the 1σ formal uncertainty in the asteroid's GM as a function of asteroid radius and bulk density, for the baseline flyby configuration at 50 m altitude above the surface, 5 km/s, involving two GIRO spacecraft and expected performance GIRO Doppler noise. The color scale indicates the magnitude of the GM relative uncertainty

The results show that, without APIC imaging, meaningful mass estimation is not achievable. When images are included, a relative GM uncertainty better than 30% is obtained only for asteroids with diameters of approximately 300 m or larger. This confirms that Earth-based tracking alone, under typical flyby conditions, is insufficient for precise mass determination of small bodies and depends heavily on favorable geometry–conditions that may be difficult to guarantee in the context of rapid reconnaissance missions for planetary defense. In contrast, the inclusion of GIRO beacons enables high-accuracy mass estimation across a broad range of asteroid sizes, down to radii as small as 30 m. In this configuration, the GM uncertainty remains below 25% for all tested cases and drops below 1% for asteroids with radii larger than approximately 130 m.

Figure 15 provides a contour plot for the two-GIRO configuration, showing the 1σ GM uncertainty as a function of asteroid radius (30–500 m) and bulk density (1.0–6.0 g/cm^3), using the baseline flyby scenario. The results indicate that, for asteroids larger than 100–150 m in radius, density has a limited effect on the uncertainty, with accuracies below 1%. However, for smaller bodies, the influence becomes more pronounced. For example, for a 30 m radius asteroid, the uncertainty scales linearly with density, as expected, and ranges from approximately 28% at 1.0 g/cm^3 to 5% at 6.0 g/cm^3.

These findings confirm the potential of the GIRO system to enable reliable mass estimation across a wide range of flyby conditions, including small, fast, and low-density targets.

8 Conclusions

This study provides a comprehensive performance assessment of the Gravity Imaging Radio Observer concept for precise mass estimation of small asteroids during close flybys, leveraging high-precision inter-satellite Doppler tracking combined with optical imaging. Using a detailed simulated flyby of the 60-meter asteroid 2024 YR4 as a rep-

resentative case, assuming a low Bennu-like density, we demonstrate that a dual-beacon configuration with Doppler noise levels in the range of 1.0 to 0.1 μm/s enables unprecedented accuracy in estimating the asteroid's gravitational parameter during a flyby. In this work, the specific onboard guidance algorithm that ensures the correct execution of the close flyby is not simulated, as such modeling lies beyond the scope of this study and its effectiveness has already been demonstrated in previous missions. Nevertheless, the execution uncertainties of the terminal guidance navigation maneuvers are incorporated into our dynamical model, as they affect the flyby geometry and, consequently, the achievable GM accuracy.

Under realistic conditions involving moderate relative velocities and challenging flyby geometries, GIRO achieves relative uncertainties in the order of 20%, with performance improving to a few percent uncertainty for encounter velocities near 1 km/s. We then expanded the analysis showing robust mass estimates across a wide range of asteroid sizes, densities, number of GIROs, and flyby geometries.

The results highlight several key findings:

- A host spacecraft-only flyby configuration, even when supported by dual-link Doppler from Earth, WVR calibration, and optimal Earth-view geometry, enables meaningful GM estimation only for asteroids larger than approximately 150 m in radius, assuming a Bennu-like density.
- The GIRO release direction analysis highlighted that releasing the beacons along the cross-track direction yields the best GM results, whereas an along-track release results in a significant loss of GM observability.
- A single GIRO, combined with optical imaging, is sufficient to enable accurate mass estimation for asteroids with radii as small as 30 m when released in an optimal geometry (e.g., co-aligned with the host spacecraft at closest approach). Adding a second and third beacon further improves the solution, providing up to a factor of 1.6 reduction in the GM uncertainty compared to the single-GIRO case–yielding relative accuracies on the order of 20%–and is also recommended to enhance redundancy and overall robustness.
- Asteroid images acquired within a few minutes of closest approach are not critical for mass estimation. However, they significantly improve the heliocentric orbit determination of the asteroid, as well as the relative positioning of the spacecraft and GIROs.
- The GIRO experiment estimates the asteroid's mass using only relative measurements, making the GM determination independent of Earth-based tracking. Nonetheless, Earth-based data remain important for constraining the asteroid's ephemeris.
- Post-flyby data carry the highest information content, with the differential deflection between the host spacecraft and the beacons providing the strongest signal. Even without data exactly at closest approach, precise GM estimation remains achievable.
- The impact of the last terminal guidance maneuver execution on GM uncertainty ranges from 20% when the maneuver is performed at CA–30 min to 42% when executed at CA–5 min. For the flyby configuration considered in this study, the final maneuver is expected at CA–20 min, leading to a mass uncertainty of $\sim$ 20%. Regarding spacecraft attitude control, for flyby velocities exceeding 5 km/s, maintaining an inertially fixed attitude around closest approach–thereby avoiding rapid slews–is recommended to reduce the influence of unmodeled non-gravitational accelerations.

- Increasing host spacecraft stochastic acceleration outside the CA window from the nominal 10^{-12} km/s^2 up to 10^{-10} km/s^2 has a negligible impact on GM estimation accuracy. Stochastic accelerations acting on the beacons have an even smaller impact on GM estimation. Moreover, if needed, their effects can be mitigated by modeling correlations due to the identical geometry of the beacons. The GIRO design as a spinner, having its spin axis oriented normal to the spacecraft–GIRO relative velocity, averages out spacecraft thermal re-radiation in the plane perpendicular to the spin axis. When two GIROs are flown simultaneously, residual common-mode components along the spin axis can also be effectively canceled through differential measurements.
- The GIRO-based mass-estimation approach is scalable across a broad range of flyby conditions. For example, under a two-beacon configuration and assuming GIRO expected-performance Doppler noise, the method yields relative GM uncertainties below 47% at 10 km/s and 50 m altitude for a Bennu-like density 2024 YR4, about 23% at 5 km/s, and as low as 5% for 1 km/s flybys. For the fast flybys, the addition of a third GIRO further reduces the uncertainties by a factor of approximately 1.3.
- The method is robust to variations in asteroid size and density. For a 50 m altitude above the surface, 5 km/s flyby of a 1.0 g/cm^3 asteroid, the relative GM uncertainty is about 28% for a 30 m radius object, and below 1% for radii larger than ∼150 m. Sensitivity to bulk density becomes significant only for very small asteroids (e.g., 30 m radius), with GM uncertainties around 28% for low-density bodies (1.0 g/cm^3), improving to 5% for high-density cases (6.0 g/cm^3). For asteroids larger than 100 m, the results are largely insensitive to density variations.
- The system is well-suited for rapid-response missions, as it requires no ground-based geometric constraints and can leverage COTS components for fast and flexible deployment.

Overall, the GIRO concept emerges as a flexible, cost-effective, and highly promising technology for enabling precise mass estimation of small asteroids under a wide range of flyby conditions, including variations in encounter velocity, geometry, and target properties such as size and density. By delivering high-accuracy, Earth-independent measurements through inter-satellite Doppler tracking, GIRO overcomes many of the limitations of traditional methods and extends gravity science to objects that were previously inaccessible during flybys. This capability is particularly valuable for planetary defense–where rapid, robust, and accurate characterization of potential threats is essential.

Acknowledgements This work was carried out at the Jet Propulsion Laboratory, California Institute of Technology, under a contract with the National Aeronautics and Space Administration (80NM0018D0004). Government sponsorship acknowledged. © 2025. All rights reserved. EG, AM, PT, and MZ wish to acknowledge Caltech and the NASA Jet Propulsion Laboratory for granting the University of Bologna a license to an executable version of MONTE Project Edition S/W. The Crameri [15] scientific colour maps are used in this study to prevent visual distortion of the data and exclusion of readers with colour-vision deficiencies [17].

Author Contributions E.G. performed the simulations, prepared the figures, worked on methodology and wrote the manuscript. R.P. supervised the project and contributed to conceptualization, methodology, and manuscript review. J.R. assisted with conceptualization, methodology, and manuscript editing. A.M. verified simulations and contributed to manuscript editing. S.C. and D.F. contributed to methodology and manuscript review-editing. P.T. and M.Z. reviewed the manuscript. All authors approved the final version.

Funding EG, AM, PT, and MZ are grateful to the Italian Space Agency (ASI) for financial support through Agreement No. 2022-8-HH.0 in the context of ESA's Hera mission, ASI contract n. 2023-18-I.0 "Asteroid Nodal Intersection Multiple Encounters (ANIME)", and ASI contract n. 2024-49-I.0 "Phase A Study for Robotic Asteroid Exploration (NEA) Missions".

Data Availability No datasets were generated or analysed during the current study.

Declarations

Conflict of interest The authors declare no conflict of interest.

References

1. Asmar, S.W., Armstrong, J.W., Iess, L., Tortora, P.: Spacecraft doppler tracking: noise budget and accuracy achievable in precision radio science observations. Radio Sci. **40**(2), 1–9 (2005). https://doi.org/10.1029/2004RS003101
2. A'Hearn, M.F., Belton, M.J.S., Delamere, W.A., Kissel, J., Klaasen, K., McFadden, L.A., White, A.R.: Deep impact: excavating comet Tempel 1. Science **310**(5746), 258–264 (2005)
3. Abich, K., Braxmaier, C., Gohlke, M., Sanjuan, J., Abramovici, A., Okihiro, B., et al.: In-orbit performance of the grace follow-on laser ranging interferometer. Phys. Rev. Lett. **123**, 031101 (2019). https://doi.org/10.1103/PhysRevLett.123.031101
4. Atchison, J.A., Mitch, R.H., Apland, C., Kee, C.L., Harclerode, K.W.: Small body in-situ multi-probe mass estimation experiment (SIMMEE). In: 2017 IEEE Aerospace Conference, pp. 1–9. IEEE (2017)
5. Atchison, J.A., Mitch, R.H., Mazarico, E.: Optical gravimetry for flyby missions: parametric study and validation. In: Lunar and Planetary Science Conference, vol. 48 (2017)
6. Bull, R., Atchison, J., Bradfield, J., Woodburn, J.: Hypothetical asteroid 2023 PDC mass measurement via doppler gravimetry in a reconnaissance flyby. Acta Astronaut. **214**, 619–628 (2024)
7. Bellerose, J., Bhaskaran, S., Rush, B., Tarzi, Z., Velez, D., Mages, D., Vaughan, A., Laipert, F., Atchison, J., McQuaide, M., et al.: Double asteroid redirection test (DART): navigating to obliteration. Acta Astronaut. **219**, 417–427 (2024)
8. Buys, M., Hanner, C.P., Barbee, B.W.: Refining asteroid mass uncertainty via volume and bulk density constraints for optimal flyby mission design. In: 9th IAA Planetary Defense Conference (2025)
9. Bolin, B.T., Hanuš, J., Denneau, L., Bonamico, R., Abron, L.-M., Delbo, M., Durech, J., Jedicke, R., Alcorn, L.Y., Cikota, A., et al.: The discovery and characterization of earth-crossing asteroid 2024 YR4. Astrophys. J. Lett. **984**(1), 25 (2025)
10. Buccino, D., Kahan, D., Parisi, M., Paik, M., Barbinis, E., Yang, O., Park, R., Tanner, A., Bryant, S., Jongeling, A.: Performance of earth troposphere calibration measurements with the advanced water vapor radiometer for the Juno gravity science investigation. Radio Sci. **56**(12), 1–9 (2021)
11. Cheng, A.F., Atchison, J., Kantsiper, B., Rivkin, A.S., Stickle, A., Reed, C., et al.: Asteroid impact and deflection assessment mission. Acta Astronaut. **115**, 262–269 (2015)
12. Chesley, S.R., Chodas, P.W., Milani, A., Valsecchi, G.B., Yeomans, D.K.: Quantifying the risk posed by potential earth impacts. Icarus **159**(2), 423–432 (2002). https://doi.org/10.1006/icar.2002.6910

13. Chesley, S.R., French, A.S., Davis, A.B., Jacobson, R.A., Brozovic, M., Farnocchia, D., Lauretta, D.S.: Trajectory estimation for particles observed in the vicinity of (101955) Bennu. J. Geophys. Res. Planets **125**(9), e2019JE006363 (2020)
14. Christensen, L., Park, R.S., Bell, J.F., III.: Estimating asteroid mass from optically tracked radio beacons. J. Spacecr. Rocket. **58**(2), 444–455 (2021)
15. Crameri, F.: Scientific colour maps. Zenodo **10**, 5281 (2018). https://doi.org/10.5281/zenodo.1243862
16. Cheng, A.F., Rivkin, A.S., Michel, P., Atchison, J., Barnouin, O., Benner, L., Chabot, N.L., Ernst, C., Fahnestock, E.G., Kueppers, M., et al.: AIDA DART asteroid deflection test: planetary defense and science objectives. Planet. Space Sci. **157**, 104–115 (2018)
17. Crameri, F., Shephard, G.E., Heron, P.J.: The misuse of colour in science communication. Nat. Commun. **11**, 5444 (2020). https://doi.org/10.1038/s41467-020-19160-7
18. Evans, S., Taber, W., Drain, T., Smith, J., Wu, H.-C., Guevara, M., Sunseri, R., Evans, J.: MONTE: the next generation of mission design and navigation software. CEAS Space J. **10**(1), 79–86 (2018)
19. Farnocchia, D., Fenucci, M., Bernardi, F., et al.: The impact hazard assessment for near-Earth asteroid 2024 YR$_4$. J. Astronaut. Sci. **73** (2026). https://doi.org/10.1007/s40295-026-00576-0
20. Frauenholz, R.B., Bhat, R.S., Chesley, S.R., Mastrodemos, N., Owen, W.M., Jr., Ryne, M.S.: Deep impact navigation system performance. J. Spacecr. Rocket. **45**(1), 39–56 (2008)
21. Gramigna, E., Johansen, J.G., Manghi, R.L., Magalhães, J., Zannoni, M., Tortora, P., et al.: Hera inter-satellite link doppler characterization for didymos gravity science experiments. In: 2022 IEEE 9th International Workshop on Metrology for AeroSpace (MetroAeroSpace), pp. 430–435. IEEE (2022)
22. Granvik, M., Morbidelli, A., Jedicke, R., Bolin, B., Bottke, W.F., Beshore, E., Vokrouhlický, D., Delbó, M., Michel, P.: Debiased orbit and absolute magnitude distributions for near-earth objects. Astron. Astrophys. **618**, 61 (2018). https://doi.org/10.1016/j.icarus.2018.04.018
23. Gramigna, E., Manghi, R.L., Zannoni, M., Tortora, P., Park, R.S., Tommei, G., Le Maistre, S., Michel, P., Castellini, F., Kueppers, M.: The Hera radio science experiment at Didymos. Planet. Space Sci. **246**, 105906 (2024)
24. Housen, K.R., Holsapple, K.A.: Ejecta from impact craters. Icarus **211**(1), 856–875 (2011). https://doi.org/10.1016/j.icarus.2010.09.017
25. Holsapple, K.A.: About deflecting asteroids and comets. In: Proceedings of the Planetary Defense Conference: Protecting Earth from Asteroids (2004)
26. Hesar, S., Parker, J., Mcmahon, J., Born, G.: Small body gravity field estimation using liaison supplemented optical navigation. In: AAS GN&C Conference (2015)
27. International Asteroid Warning Network (IAWN): Final Notification: Probability of Impact of Near-Earth Asteroid 2024 YR4 on 22 December 2032. (2025) https://iawn.net/documents/NOTIFICATIONS/2024-YR4_IAWN_Final-Notification_20250224.pdf. Accessed 24 Feb 2025
28. Kizner, W.: A method of describing miss distances for lunar and interplanetary trajectories. Planet. Space Sci. **7**, 125–131 (1961)
29. Konopliv, A.S., Park, R.S., Yuan, D.-N., Asmar, S.W., Watkins, M.M., Williams, J.G., Fahnestock, E., Kruizinga, G., Paik, M., Strekalov, D., et al.: High-resolution lunar gravity fields from the grail primary and extended missions. Geophys. Res. Lett. **41**(5), 1452–1458 (2014)
30. Lehman, D.H., Hoffman, T.L., Havens, G.G.: The Gravity Recovery and Interior Laboratory mission. In: 2013 IEEE Aerospace Conference, Big Sky, MT, USA, 2013, pp. 1–11. https://doi.org/10.1109/AERO.2013.6496866
31. Lauretta, D.S., Balram-Knutson, S.S., Beshore, E. et al.: OSIRIS-REx: sample return from asteroid (101955) Bennu. Space Sci. Rev. **212**, 925–984 (2017). https://doi.org/10.1007/s11214-017-0405-1
32. Landerer, F., Flechtner, F., Wiese, D., et al.: Extending the global mass change data record: GRACE follow-on. Geophys. Res. Lett. **47**, e2020GL088306 (2020). https://doi.org/10.1029/2020GL088306
33. Levison, H.F., Olkin, C.B., Noll, K.S., Marchi, S., Bell, J.F., III., Bierhaus, E., Binzel, R., Bottke, W., Britt, D., Brown, M., Buie, M.: Lucy mission to the trojan asteroids: science goals. Planet. Sci. J. **2**(5), 171 (2021)
34. Mainzer, A., Bauer, J., Grav, T., Masiero, J., Cutri, R.M., Dailey, J., Eisenhardt, P., McMillan, R.S., Wright, E.L., Walker, R.G., Jedicke, R., Spahr, T.: NEOWISE observations of near-earth objects: Preliminary results. Astrophys. J. **743**(2), 156 (2011). https://doi.org/10.1088/0004-637X/743/2/156
35. Mastrodemos, N., Kubitschek, D.G., Synnott, S.P.: Autonomous navigation for the Deep Impact mission encounter with comet Tempel 1. Space Sci. Rev. **117**, 95–121 (2005)
36. Moyer, T.D.: Mathematical formulation of the double precision orbit determination program/dpodp. Technical Report JPL-TR-32-1527, Jet Propulsion Laboratory (1971)

37. Moyer, T.D.: Formulation for Observed and Computed Values of Deep Space Network Data Types for Navigation. John Wiley & Sons (2005)
38. NASA-JPL-SSD: Solar System Dynamics. (2025) https://ssd.jpl.nasa.gov/tools/sbdb_lookup.html#/?sstr=2024%20YR4. Information retrieved on June 2025
39. National Research Council: Defending Planet Earth: Near-Earth Object Surveys and Hazard Mitigation Strategies. The National Academies Press, Washington, DC (2010). https://doi.org/10.17226/12842
40. Park, R.S., Asmar, S.W., Fahnestock, E.G., Konopliv, A.S., Lu, W., Watkins, M.M.: Gravity recovery and interior laboratory simulations of static and temporal gravity field. J. Spacecr. Rocket. **49**(2), 390–400 (2012). https://doi.org/10.2514/1.A32117
41. Pätzold, M., Andert, T., Hahn, M., Asmar, S., Barriot, J.-P., Bird, M., Häusler, B., Peter, K., Tellmann, S., Grün, E., et al.: A homogeneous nucleus for comet 67P/Churyumov–Gerasimenko from its gravity field. Nature **530**(7588), 63–65 (2016)
42. Park, R.S., Folkner, W.M., Williams, J.G., Boggs, D.H.: The JPL planetary and lunar ephemerides DE440 and DE441. Astron. J. **161**(3), 105 (2021)
43. Park, R., Jacobson, R., Gomez Casajus, L., Nimmo, F., Ermakov, A., Keane, J., McKinnon, W., Stevenson, D., Akiba, R., Idini, B., et al.: Io's tidal response precludes a shallow magma ocean. Nature **638**(8049), 69–73 (2025)
44. Park, R.S., Konopliv, A.S., Bills, B.G., Rambaux, N., Castillo-Rogez, J.C., Raymond, C.A., Vaughan, A.T., Ermakov, A.I., Zuber, M.T., Fu, R.R., Toplis, M.J., Russell, C.T., Nathues, A., Preusker, F.: A partially differentiated interior for ceres deduced from its gravity field and shape. Nature **537**, 515–517 (2016). https://doi.org/10.1038/nature18955
45. Park, R., Riedel, J., Brandon, E., Harvey, N., Manafi, S., Smart, M., Towfic, Z., Berne, A., Bertiger, W., Keane, J., et al.: Gravity Imaging Radio Observer (GIRO) for planetary science and mission opportunities. Planet. Sci. J. **6**(5), 127 (2025)
46. Park, R.S., Riedel, J.E., Ermakov, A.I., Roa, J., Castillo-Rogez, J., Davies, A.G., McEwen, A.S., Watkins, M.M.: Advanced Pointing Imaging Camera (APIC) for planetary science and mission opportunities. Planet. Space Sci. **194**, 105095 (2020)
47. Rivkin, A.S., Chodas, P.W., Cheng, A.F., Michel, P., Stickle, A.M., Thomas, C.A., et al.: The DART mission: planetary defense investigations and requirements. Planet. Sci. J. **2**(4), 173 (2021). https://doi.org/10.3847/PSJ/ac063e
48. Rivkin, A., Mueller, T., MacLennan, E., Holler, B., Burdanov, A., Wit, J., Pravec, P., Micheli, M., Devogele, M., Conversi, L., et al.: JWST observations of potentially hazardous asteroid 2024 YR4. Res. Notes AAS **9**(4), 70 (2025)
49. Scheeres, D., French, A., Tricarico, P., Chesley, S., Takahashi, Y., Farnocchia, D., McMahon, J., Brack, D., Davis, A., Ballouz, R.-L., et al.: Heterogeneous mass distribution of the rubble-pile asteroid (101955) Bennu. Sci. Adv. **6**(41), 3350 (2020)
50. Scheeres, D.J., McMahon, J.W., French, A.S., Brack, D.N., Chesley, S.R., Farnocchia, D., Takahashi, Y., Leonard, J.M., Geeraert, J., Page, B., Antreasian, P.: The dynamic geophysical environment of (101955) Bennu based on OSIRIS-REx measurements. Nat. Astron. **3**(4), 352–361 (2019)
51. Syal, M.B., Owen, J.M., Miller, P.L.: Deflection by kinetic impact: sensitivity to asteroid properties. Icarus **269**, 50–61 (2016)
52. Sergeyevsky, A.B., Snyder, G.C., Cunniff, R.A.: Interplanetary Mission Design Handbook. Earth to Mars Ballistic Mission Opportunities, 1990-2005 vol. I, part 2, p. 20. NASA/JPL, (1983). JPL Publication 82-43. https://ntrs.nasa.gov/citations/19840010158
53. Taylor, M.G.G.T., Altobelli, N., Buratti, B.J., Choukroun, M.: The Rosetta mission orbiter science overview: the comet phase. Philos. Trans. R. Soc. A Math. Phys. Eng. Sci. **375**(2097), 20160262 (2017)
54. Thornton, C.L., Border, J.S.: Radiometric Tracking Techniques for Deep-Space Navigation. John Wiley & Sons (2003)
55. Tapley, B.D., Bettadpur, S., Watkins, M., Reigber, C.: The gravity recovery and climate experiment: mission overview and early results. Geophys. Res. Lett. **31**, L09607 (2004). https://doi.org/10.1029/2004GL019920
56. Tsuda, Y., Saiki, T., Terui, F., Nakazawa, S., Yoshikawa, M., Watanabe, S.I., Team, H.P: Hayabusa2 mission status: landing, roving and cratering on asteroid Ryugu. Acta Astronaut. **171**, 42–54 (2020)
57. Yoshikawa, M., Kawaguchi, J., Fujiwara, A., Tsuchiyama, A.: Hayabusa sample return mission. In: DeMeo, F.E., Bottke, W.F. (eds.) Asteroids IV. University of Arizona Press, Tucson, pp. 397–418 (2015)

58. Zuber, M., Smith, D., Lehman, D., et al.: Gravity Recovery and Interior Laboratory (GRAIL): mapping the lunar interior from crust to core. Space Sci. Rev. **178**, 1–30 (2013). https://doi.org/10.1007/s11214-012-9952-7
59. Zuber, M.T., Smith, D.E., Neumann, G.A., Goossens, S., Andrews-Hanna, J.C., Head, J.W., Kiefer, W.S., Asmar, S.W., Konopliv, A.S., Lemoine, F.G., Matsuyama, I., Melosh, H.J., McGovern, P.J., Nimmo, F., Phillips, R.J., Solomon, S.C., Taylor, G.J., Watkins, M.M., Wieczorek, M.A., Williams, J.G., Goossens, S.J., Kruizinga, G., Mazarico, E., Park, R.S., Yuan, D.-N.: Gravity field of the orientale basin from the Gravity Recovery and Interior Laboratory (GRAIL) mission. Science **354**(6311), 438–441 (2016). https://doi.org/10.1126/science.aag0519

Authors and Affiliations

Edoardo Gramigna[1,2] · Ryan S. Park[1] · Joseph E. Riedel[1] · Andrea Magnanini[1,3] · Steven R. Chesley[1] · Davide Farnocchia[1] · Paolo Tortora[2,3] · Marco Zannoni[2,3]

✉ Edoardo Gramigna
edoardo.gramigna@unibo.it

Ryan S. Park
ryan.s.park@jpl.nasa.gov

Joseph E. Riedel
joseph.e.riedel@jpl.nasa.gov

Andrea Magnanini
andrea.magnanini3@unibo.it

Steven R. Chesley
steve.chesley@jpl.nasa.gov

Davide Farnocchia
davide.farnocchia@jpl.nasa.gov

Paolo Tortora
paolo.tortora@unibo.it

Marco Zannoni
m.zannoni@unibo.it

[1] Jet Propulsion Laboratory, California Institute of Technology, Pasadena, CA 91011, USA

[2] Centro Interdipartimentale di Ricerca Industriale Aerospaziale, Alma Mater Studiorum - Università di Bologna, 47121 Forlí, FC, Italy

[3] Department of Industrial Engineering, Alma Mater Studiorum - Università di Bologna, 47121 Forl'i, FC, Italy